Atmos. Chem. Phys. Discuss., https://doi.org/10.5194/acp-2019-288
Manuscript under review for journal Atmos. Chem. Phys.
Discussion started: 12 April 2019

Atmospheric Chemistry and Physics Discussions

The ice-nucleating ability of quartz immersed in water and its atmospheric importance compared to K-feldspar

Alexander D. Harrison[1], Katherine Lever[1], Alberto Sanchez-Marroquin[1], Mark A. Holden[1,2*], Thomas F. Whale[1,2], Mark D. Tarn[1], James B. McQuaid[1] and Benjamin J. Murray[1]

[1]School of Earth and Environment, University of Leeds, Leeds, LS2 9JT, UK
[2]School of Chemistry, University of Leeds, Leeds, LS2 9JT, UK
* Now at School of Physical Sciences and Computing, University of Central Lancashire, Preston PR1 2HE, UK

Abstract. Mineral dust particles are thought to be an important type of ice-nucleating particle (INP) in the mixed-phase cloud regime around the globe. While K-feldspar has been identified as being a particularly important component of mineral dust for ice nucleation, it has been shown that quartz is also relatively ice nucleation active. Given quartz typically makes up a substantial proportion of atmospheric desert dust it could potentially be important for cloud glaciation. Here, we survey the ice-nucleating ability of 10 α-quartz samples (the most common quartz polymorph) when immersed in microlitre supercooled water droplets. Despite all samples being α-quartz, the temperature at which they induce freezing varies by around 12°C for a constant active site density. We find that some quartz samples are very sensitive to ageing in both aqueous suspension and air, resulting in a loss of ice-nucleating activity, while other samples are insensitive to exposure to air and water over many months. The sensitivity to water and air is perhaps surprising as quartz is thought of as a chemically resistant material, but this observation suggests that the active sites responsible for nucleation are less stable than the bulk of the material. We find that the quartz group of minerals are generally less active than K-feldspars, although the most active quartz samples are of a similar activity to some K-feldspars. We also find that the quartz samples are generally more active than the plagioclase feldspar group of minerals and the albite end-member has an intermediate activity. Using both the new and literature data, active site density parameterisations have been proposed for quartz, K-feldspar, plagioclase and albite. Combining these parameterisations with the typical atmospheric abundance of each mineral and comparing the results with atmospheric ice-nucleating particle concentrations, supports previous work that suggests that K-feldspar dominates, rather than quartz (or other minerals), the ice nucleation particle population in desert dust aerosol.

Atmos. Chem. Phys. Discuss., https://doi.org/10.5194/acp-2019-288
Manuscript under review for journal Atmos. Chem. Phys.
Discussion started: 12 April 2019

Atmospheric Chemistry and Physics Discussions

1 Introduction

The formation of ice in supercooled clouds strongly affects hydrometeor size which in turn impacts cloud lifetime, precipitation and radiative properties (Kanji et al., 2017; Murray et al., 2012). There are a number of primary and secondary mechanisms through which ice can form in clouds. Homogeneous freezing of cloud droplets becomes increasingly important below -33 °C (Herbert et al., 2015), but clouds commonly glaciate at much warmer temperatures (Ansmann et al., 2009; Kanitz et al., 2011). Freezing at these warmer temperatures can occur through secondary ice production (Field et al., 2016) or heterogeneous freezing on ice-nucleating particles (INPs) (Hoose and Mohler, 2012). The presence of INPs, which tend to comprise only a small fraction of cloud condensation nuclei, can dramatically reduce the lifetime of shallow clouds (Vergara-Temprado et al., 2018), and alter the development of deep convective clouds through, for example, the release of latent heat which invigorates the updraft thus altering cloud structure (Lohmann, 2017; Rosenfeld et al., 2011). It is also recognised that an accurate representation of cloud phase is important for assessments of climate sensitivity (Tan et al., 2016). However, our understanding of which aerosol types serve as effective INPs in the mixed phase regime is incomplete.

Mineral dust has been inferred to be an effective INP in the atmosphere from field, model and laboratory studies (Hoose and Möhler, 2012; Vergara-Temprado et al., 2017). Observations of aerosol at the centre of ice crystals have shown that mineral dust is often present, suggesting they act as INPs (Eriksen Hammer et al., 2018; Iwata and Matsuki, 2018; Pratt et al., 2009). Laboratory studies also demonstrate mineral dusts are relatively effective at nucleating ice (DeMott et al., 2015; Hoose and Möhler, 2012; Murray et al., 2012). Atmospheric mineral dusts are composed of several components and until relatively recently work focused on the clay group of minerals for ice nucleation studies since clay is the major component of airborne mineral dust and is sufficiently small that its atmospheric lifetime is relatively long (Broadley et al., 2012; Mason and Maybank, 1958; Murray et al., 2011; Pinti et al., 2012; Roberts and Hallett, 1968; Wex et al., 2014). However, more recent work shows that K-rich feldspars (K-feldspars) are very effective ice nucleants when immersed in supercooled water (Atkinson et al., 2013; DeMott et al., 2018; Harrison et al., 2016; Niedermeier et al., 2015; Peckhaus et al., 2016; Reicher et al., 2018; Tarn et al., 2018; Whale et al., 2017; Zolles et al., 2015). However, there are other minerals present in the atmosphere, many of which are relatively poorly characterised in terms of their ice-nucleating activity.

Quartz is a major component of aerosolised atmospheric mineral dust (Glaccum and Prospero, 1980; Perlwitz et al., 2015) and studies have shown that it can be active as an INP (Atkinson et al., 2013; Holden et al., 2019; Isono and Ikebe, 1960; Kumar et al., 2018; Zolles et al., 2015). Boose et al. (2016) showed a correlation between the INP activity of nine desert dusts and the concentration of K-feldspar at temperatures of -20.15 °C. However, at lower temperatures (-35.15 to -28.15 °C) the ice-nucleating activity of the dusts correlated with the combined concentration of quartz and K-feldspar. Boose et al. (2016) thus emphasised the importance of understanding quartz and feldspars present in the atmosphere for the modelling of INPs. Recently, Kumar et al. (2018) investigated five quartz samples (two synthetic, three naturally occurring) for their ice-nucleating activity. They demonstrated the activity of quartz as well as its susceptibility to ageing in pure water and solute suspensions. In addition, several authors relate the milling process of quartz to its ice-nucleating ability and suggest that defects created as a result of milling act as ice active sites (Kumar et al., 2018; Zolles et al., 2015). Kumar et al. (2018) showed that these sites were sensitive to ageing and they suggest that they are susceptible to dissolution. Very recently, Holden et al. (2019) demonstrated that nucleation on quartz is indeed site specific, through repeat freezing experiments with high-speed cryomicroscopy, and found that micron sized defects tended to be collocated with the nucleation sites. While our understanding of ice nucleation by quartz has improved recently, it is still unclear quite how variable quartz samples are in their ice-nucleating ability, which prevents an assessment of its atmospheric importance as an ice-nucleating material relative to other minerals.

We present a survey of the ice-nucleating ability of 10 naturally occurring quartz samples and demonstrate the variability in ice-nucleating ability within natural quartz. We also explore the stability of a subset of these samples to time spent in water or air. Then, in order to compare the potential contribution of quartz to the atmospheric INP population to that of other minerals we have generated a parameterisation for quartz based on the experimental work in this study. In addition we present new parameterisations for K-feldspar, plagioclase feldspar, and albite feldspar based on datasets available in the literature. This allows us to compare the potential contribution of quartz, albite, plagioclase and K-feldspar to the atmospheric INP population.

2 Quartz, the mineral

Quartz is the second most abundant mineral in the Earth's crust after the feldspar group of minerals. Its hardness (Moh's scale 7) and chemical nature along with its lack of cleavage planes mean it is also a common constituent of sands and soils as it is resistant to weathering processes. Although quartz does not have cleavage planes it does exhibit conchoidal fracturing meaning particles tend to have smoothly curving surfaces as a result of fracturing (Deer et al., 1966), rather than planes with steps that might be expected on a cleavage plane. As it is a common constituent to soils, including desert soils, it can be lofted into the atmosphere and is found within transported mineral dusts (Avila et al., 1997; Caquineau et al., 1998; Kandler et al., 2009; Kandler et al., 2011).

The silica minerals are composed of SiO_2 tetrahedra with each silicon being bonded to four oxygen atoms and these tetrahedra form a 3D framework which can be in six or eight membered loops (Deer et al., 1992). There are three principle crystalline types of SiO_2: quartz, cristobalite and tridymite, with stishovite and coesite being other high pressure polymorphs. The polymorph that is present depends on the temperature and pressure during formation (Koike et al., 2013; Swamy et al., 1994). All three crystalline silica types (quartz, cristobalite and tridymite) can exist in two polymorphs, both a high temperature (β) and low temperature (α) state. α-quartz is most commonly found at or near the Earth's surface due to it being the most stable at atmospheric conditions and thus is the dominant polymorph of quartz found in soils and in atmospheric desert dust aerosol. In fact, α-quartz is so common that by convention it is referred to simply as quartz.

Generally, quartz samples tend to be close to 100 % SiO_2 although it is common to find small amounts of oxides as inclusions or liquid infillings within cavities (Deer et al., 1966). The substitution of Al^{3+} for Si^{4+} allows for the introduction of alkali ions such as Li^+ and Na^+. These subtle impurities can lead to a variety of colours. If quartz with impurities (for example Al) is exposed to low levels of naturally occurring radiation then one pair of electrons from an oxygen adjacent to Al can be emitted leaving unpaired electrons otherwise known as "hole defects" (Nassau, 1978). This forms the basis for colour centres, which cause the colouration of amethyst. Amethyst is typically violet in colour and differs from standard α-quartz in that it has a larger proportion of Fe_2O_3 inclusions and marginally more TiO_2 and Al_2O_3 in its structure (Deer et al., 1966). Rose quartz generally contains higher amounts of alkali oxides, TiO_2, Fe_2O_3, TiO_2 and MnO_2 (Deer et al., 1966). It has a pinkish colour which is thought to be attributed to the presence of a fibrous mineral which was first suggested to be dumortierite (Applin and Hicks, 1987; Kibar et al., 2007) but has been suggested to be a different, unclassified type of mineral (Goreva et al., 2001). Smoky quartz has a black colour which is caused by colour centres created by the irradiation of iron (Nassau, 1978). Chalcedony is a form of cryptocrystalline or microcrystalline α-quartz (Deer et al., 1966). It has been suggested that it is also commonly intergrown with another polymorph of quartz known as moganite (Götze et al., 1998; Heaney and Post, 1992). Moganite has a monoclinic crystal structure opposed to the trigonal crystal system of quartz. Chalcedony often includes micropores within its structure due to its microcrystalline nature (Deer et al., 1966).

3 Materials and Methods

3.1 Samples and preparation

10 α-quartz samples were tested for their ice-nucleating ability. These included four typical α-quartzes, two amethysts, two microcrystalline quartzes (chalcedony), one rose quartz and one smoky quartz, as summarised in Table 1. Photographs of the samples are presented in Figure 1. These samples were selected to investigate the natural variability of the ice-nucleating ability of α-quartz.

These samples were sourced from various gem sellers. The minerals were visually inspected, using their colour, crystal habit, lustre and cleavage to confirm whether the mineral was quartz and, if so, what type of quartz. Rietveld refinement of powder X-ray diffraction (XRD) patterns was then used to verify the silica polymorph and identify any significant crystalline impurities. The results of this process are presented in Table 1. Raman spectroscopy was used in conjunction with XRD to test for the presence of moganite within the two chalcedony samples based on the work of Götze et al. (1998). However, both methods indicated that no moganite was present above the limit of detection (~1 wt%).

Eight of the samples were prepared from bulk rock or crystal samples by first rinsing the rock surface with isopropanol and pure water and placing in a clean sealed plastic bag before chipping off fragments and then grinding them into a powder with an agate mortar and pestle. The mortar and pestle were cleaned before use by scrubbing them with quartz sand (Fluka) and rinsing thoroughly with pure deionised water and isopropanol. A

similar method was employed by Harrison et al. (2016) who investigated less ice-active materials (plagioclase feldspars) and found that contamination from the cleaning process was not observed. Atkinson quartz (the same quartz sample as used by Atkinson et al. (2013)) and Fluka quartz were supplied as a powder, although Atkinson quartz was originally ground via the same milling process (Atkinson et al. 2013). These were reground to ensure all samples initially had freshly exposed surfaces for ice nucleation experiments.

The specific surface areas of the quartz samples were measured using the Brunauer-Emmett-Teller (BET) N_2 adsorption method with a Micromeritics TriStar 3000 instrument (Table 1). Heating of the sample at 100 ^{0}C overnight was performed under a steady flow of dry nitrogen to evaporate any moisture in the sample before the surface area measurement. After BET analysis, 1 wt% suspensions for all the samples were prepared gravimetrically by suspending a known amount of material in purified water (18.2 MΩ cm at 25 °C) in a 10 mL glass vial. As quartz is a hard mineral the use of magnetic stirrer bars was avoided when suspending the material as preliminary experiments showed the potential for the Teflon coating to abrade off the stirrer bars and become mixed with the suspension. We also chose not to use glass stirrer bars, partly because glass is softer than quartz and partly because we have noted in the past that is can be a source of contamination. Therefore particles were suspended by vortexing for 5 mins prior to ice nucleation experiments. Only small amounts of sample were available for Mexico quartz and Uruguay amethyst and so the powder used for BET analysis was then used to prepare the suspensions for ice nucleation experiments. The BET analysis and subsequent suspension in water was carried out within a week of grinding the sample.

3.2 Ice nucleation experiments

The microlitre Nucleation by Immersed Particle Instrument (µL-NIPI) was employed to test the ice-nucleating ability of the various quartz samples in the immersion mode (Whale et al., 2015). This technique has been used in several previous ice nucleation studies e.g.(Atkinson et al., 2013; Harrison et al., 2016; O'Sullivan et al., 2014) and a study of nitric acid hydrate nucleation on meteoric material (James et al., 2018). In brief, 1 µL droplets of a suspension were pipetted onto a hydrophobic glass cover slip atop a cold plate (EF600, Asymptote, UK). During pipetting, the suspension was vigorously shaken every 10 droplets (with roughly 40 droplets per experiment) to keep the quartz particles suspended and to ensure that the amount of material in each droplet was similar. The cold plate and glass slide were then enclosed within a Perspex chamber and a digital camera was used to image the droplets. The temperature of the cold plate was decreased at a rate of 5 °C min^{-1} to 0 °C (from room temperature), then at 1 °C min^{-1} until all the droplets were frozen. Whilst cooling the system, a gentle flow of zero grade dry nitrogen (<0.2 L min^{-1}) was passed across the cold plate to reduce condensation onto the glass slide, which can cause interference between freezing droplets and the surrounding unfrozen droplets (Whale et al., 2015). As the droplets were cooled, images were recorded with the digital camera and freezing events identified in post analysis to calculate the fraction of droplets frozen as a function of temperature. A second run for each sample, with a fresh array of droplets, was performed immediately after the first experiment with approximately 1 hour between the two runs.

We assume that nucleation on quartz occurs at specific active sites, as supported by the work of Holden et al. (2019) who showed that nucleation occurs preferentially at specific sites on α-quartz and feldspar using high-speed cryomicroscopy of ice crystal growth on thin sections of mineral. The cumulative ice-nucleating active site density $n_s(T)$, on cooling from 0 °C to a temperature, T, was determined for each quartz sample. Standardising the active site density to the surface area of nucleant allows for comparison of the ice-nucleating ability of different materials (Connolly et al., 2009; Vali et al., 2015). It should be noted that this model neglects the time dependence of nucleation, which can have some influence on the nucleation temperature (Herbert et al., 2014; Holden et al., 2019). $n_s(T)$ is calculated using:

$$\frac{n(T)}{N} = 1 - \exp(-n_s(T)A), \qquad (1)$$

where $n(T)$ is the cumulative number of frozen droplets on cooling, N is the total number of droplets in the experiment. A is the specific surface area of nucleant per droplet calculated based on the mass of quartz per droplet (assumed to be the same as in the bulk suspension) and the surface area determined via BET analysis.

We conducted Monte Carlo simulations to estimate the error in $n_s(T)$ as a result of the randomness of the distribution of active sites in the droplet freezing experiments. These simulations consider the possible distribution of active sites throughout the droplets that explain each fraction frozen and quantify this uncertainty, which is

Atmos. Chem. Phys. Discuss., https://doi.org/10.5194/acp-2019-288
Manuscript under review for journal Atmos. Chem. Phys.
Discussion started: 12 April 2019

Atmospheric Chemistry and Physics Discussions

then combined with the uncertainty in the pipetting and BET measurements. An almost identical method was described by Harrison et al. (2016), which was similar to the work of Wright and Petters (2013).

4 Results and discussion

4.1 The variable ice-nucleating ability of α-quartz

The cumulative fraction of droplets frozen ($n(T)/N$) on cooling is shown in Fig. 2a for arrays of droplets containing the quartz samples. Comparison of these curves with the fraction frozen curves for droplets without added particles in the µL-NIPI system (Umo et al., 2015), shows that all quartz samples heterogeneously nucleate ice since the freezing temperatures for droplets containing quartz are always much higher than the pure water droplets. These fraction frozen curves are then translated into $n_s(T)$ in Fig. 2b-c. In Fig. 2b we show n_s for freshly prepared samples where the particles were suspended in water for ~10 minutes before carrying out an experiment. The variability in the ice-nucleating ability of these α-quartz samples is striking. Bombay chalcedony and Atkinson quartz are substantially more active than the other samples with the activity spanning roughly 10 °C at $n_s(T) = 10$ cm^{-2}. While the overall spread is large, it is also notable that the droplet freezing temperatures of 8 out of 10 of the samples fall between -17 °C and -20 °C at $n_s(T) = 10$ cm^{-2}.

In Fig. 2c we show n_s for both the first (fresh) run and a subsequent run performed approximately one hour after the first experiment for each quartz sample. In the cases of Bombay chalcedony, Brazil amethyst and Smokey quartz, the first and second runs where identical within the uncertainties, whereas in the other cases there was a systematic decrease in freezing temperature. For example, the temperature at which Atkinson quartz had an $n_s(T)$ of 1 cm^{-2} decreased by ~3 °C between the first experiment and the second experiment run approximately 1 h later. In the past, using this technique with mineral particles of a similar grain size has mostly resulted in consistent results from run-to-run (e.g. Atkinson et al., 2013; Whale et al., 2015). There is also consistency for some quartz samples between run to run from this study. This suggests that the decrease in activity seen for some quartz samples is a real change in the activity of the quartz rather than artefacts such as, for example, the settling of particles out of suspension leading to less surface area in each droplet. The finding that the activity of many of the α-quartz samples decrease with time spent in water is perhaps surprising given quartz is typically regarded as an inert material. We come back to this issue of ageing of active sites in water and air in section 4.2 where we describe a dedicated set of experiments to explore this issue.

The Bombay chalcedony sample stands out as being one of the most active quartz samples. For $n_s = 10$ cm^{-2} the Bombay chalcedony nucleates ice at -9 °C which is comparable to K-feldspar (see section 5.1, for a comparison with other materials). As described in section 2, chalcedony is a microcrystalline form of α-quartz and commonly has micropores. It is possible that these micropores contain ice nucleation active sites or create zones of weakness which allow defects to be created when ground. In order to test if the superior ice-nucleating ability of Bombay chalcedony is inherent to chalcedony, we located, characterised and tested a second chalcedony sample. Grape chalcedony has a similar microcrystalline form to Bombay chalcedony, but behaves more like the other quartz samples we have tested, both in having a lower ice-nucleating activity, but also in the decrease in its activity with time spent in water. One possibility is that the Bombay chalcedony sample is contaminated with another very active ice-nucleating component. The X-ray diffraction results suggest that there is not enough inorganic crystalline material, for example K-feldspar, to account for the result. In addition, we washed a ~2 g sample of unground Bombay chalcedony in 10 mL pure water (shaking vigorously for ~2 minutes) and tested the water. A droplet freezing assay with this washing water indicated that there was no significant detachable contamination. This suggests that the ice-nucleating activity of the Bombay chalcedony is inherent to the material rather than associated with an impurity, although the presence of an ice-nucleating impurity cannot be categorically excluded. These results suggests that a subtle difference between the two chalcedony samples causes the Bombay chalcedony to be much more active.

The second most active quartz sample, fresh Atkinson quartz, does not have any obvious differences with the other less active quartz samples which might explain its activity. It is almost entirely pure α-quartz with only a minor component of calcite (0.2%). It is unlikely that the calcite component is responsible for nucleation since Uruguay amethyst contains the same percent impurity of calcite and is much less ice active.

Overall, the results in Fig. 2 show a surprising diversity in ice nucleation behaviour. As mentioned above, quartz is a relatively uniform material which is chemically and physically stable, hence we might have expected its ice-

nucleating ability to be uniform and insensitive to aging processes (in fact, this was our original hypothesis when we started this project). However, the results clearly demonstrate neither of these expectations is correct. Since all these quartz samples are α-quartz we might have expected all of these quartz samples to exhibit identical nucleating properties. This variability indicates that these quartz samples do not nucleate through a lattice matching mechanism. This is consistent with the recent observation that nucleation on quartz occurs at active sites (Holden et al., 2019). Our results suggest that these active sites have diverse properties, with different activities, different site densities and some being sensitive to ageing processes where others are not. In the next section we present a set of experiments designed to further probe the aging of the ice nucleation sites on quartz samples.

4.2 The sensitivity of ice-nucleating activity with time spent in water and air

The results presented in Fig. 2 clearly indicate that the activity of many of the samples of quartz decreases by several degrees within an hour (Fig. 2b). In initial experiments we also showed that the quartz powder used by Atkinson et al. (2013) had lost its activity since it was initially tested. The sample had been stored in air within a sealed glass vial for ~5 years. However, milling of the powder dramatically increased its activity, which suggests that milling can (re)expose surfaces with the most effective active sites. This observation is similar to that described by Zolles et al. (2015) who noted that two out of three quartz samples increased in activity by up to 5 °C on milling. This supports the hypothesis that fresh surfaces are often key to maximising a quartz sample's ice-nucleating ability. Very recently, Kumar et al. (2018) have also observed that milling quartz increases its ice nucleation activity and suggest that this may be a result of defects created during the process.

In order to further explore the stability of active sites we tested how the activity of three samples of quartz varied when exposed for a range of times to water and air. For this investigation we tested: i) Smoky quartz, as it is a representative quartz in terms of its ice-nucleating ability, lying within the middle of the spread of $n_s(T)$; ii) Bombay chalcedony, as it was the most active sample and iii) Atkinson quartz, since initial experiments indicated it was highly sensitive to ageing in both water and air. The dry powder and suspension samples were stored at room temperature in a dark cupboard in sealed glass vials. Prior to the droplet freezing experiment, wet samples were agitated to re-suspend the particles and the dry powders were added to water in the standard manner described above. The $n_s(T)$ of the various quartz samples aged in both water and in air for varying times are displayed in Fig. 3.

Each of the three samples responded in a distinct manner to time spent in water. Inspection of Fig. 3 (a, c and e) reveals that while the ice-nucleating ability of Smoky quartz did not significantly decrease after ~1 h, its activity decreased by about 3 °C after four months in water. Bombay chalcedony was far more stable in water, with no substantial change in the $n_s(T)$ curve after four months, being within 1 °C of the fresh sample (close to the uncertainties of the experiment). In contrast, the activity of Atkinson quartz decreased dramatically on exposure to water. Even after only ~1 hour in suspension the $n_s(T)$ curve decreased by 2 °C, but after 16 months in water the activity decreased by 12 °C. These results point to populations of very different active sites on these three different quartz samples.

We also found that the activity of some quartz samples decreased even when they were stored in air (Fig. 3b, d and e). Dry Smoky quartz and Bombay chalcedony powders were tested after being left in a glass vial for 20 months and showed no decrease in activity. In contrast the activity of Atkinson quartz decreased by ~5 °C in half of this time period (10 months). Fig. 3f also shows the initial freezing temperatures obtained using the same sample from the Atkinson *et al.* (2013) study which had been stored for ~5 years in a glass vial. This sample was ~10 ^{0}C less active compared to the freshly ground powder.

4.3 Discussion of the nature of active sites on quartz

These results paint a complex picture of the properties of the active sites on quartz samples. Not only is the absolute activity of the samples variable, but the sensitivity of the sites to time spent in water and air is also highly variable. The active sites of the Atkinson quartz are far more susceptible to ageing in water and air than both the Smoky quartz and Bombay Chalcedony. The sites on Bombay chalcedony are stable in both air and water, whereas those on Smokey quartz are somewhat intermediate in stability, being sensitive to water only after an extended period of time beyond 1 hour.

Very recently, Kumar et al. (2018) also described the deactivation of quartz in suspension over a period of five days. However, they noted that time series experiments carried out within glass vials showed deactivation of quartz in pure water whereas experiments within polypropylene falcon tubes did not. They suggested that silicic

acid leached from the glass vial walls allows the quartz fragments to slowly grow and the active sites to be lost during the process. The explanation of Kumar et al. (2018) is consistent with our observation that the nucleating ability of many samples decreases with time spent in water. However, it is inconsistent with the stability of Bombay chalcedony and it cannot explain the loss of activity seen for Atkinson quartz when aged in air.

The physical and chemical characteristics which lead to the large variability in the properties of the ice nucleation sites on quartz are challenging to define. Classical nucleation theory suggests that ice critical clusters at the nucleation temperatures observed in this study are likely to be on the order of several nanometres across (Pummer et al., 2015). It therefore seems reasonable to think that the relevant ice nucleation sites will be on a similar scale but the nature of these sites remains unclear. A molecular dynamics study by Pedevilla et al. (2017) suggested that surfaces with strong substrate-water interaction and high densities of OH groups (or other H-bonding groups) give rise to effective sites for ice nucleation. However, sites with high densities of dangling OH groups are also inherently thermodynamically unstable and will have a tendency to either react with, for example, moisture in air, or rearrange to a more stable configuration. Hence, it may be at defects in the crystal structure where such sites become stabilised when the thermodynamic cost of having a nanoscale region with a high density of H-bonding groups is outweighed by the gain from relaxing strain in a structure. For example, in K-feldspar, it has been suggested that active sites are related to strain induced by exsolution into K and Na rich regions, which is known to result in an array of nanoscale topographical features (Whale et al., 2017). Consistent with this idea, Kiselev et al. (2016) reported that nucleation on K-feldspar was related to exposed patches of high energy (100) and Holden et al. (2019) demonstrated that nucleation on K-feldspar always occurs within micrometre scale surface imperfections. Holden et al. (2019) reports that topographic features were observed on quartz, at some of the nucleation sites, but they have not been further characterised.

Larger nanoscale patches of dangling H-bonding groups should be better at nucleating ice, but these larger high energy patches will also be less energetically stable. Hence, one might expect that the sites responsible for nucleation at the highest temperatures would also be the least stable and most sensitive to time spent in water or air. But, this does not hold for Bombay chalcedony which is the most active quartz we studied and also the most insensitive to exposure to water and air. This indicates that the sites in this case are either of a completely different chemistry (perhaps a different high energy crystal plane), or the topography and strain associated with a defect imparts a greater stability on these sites. The fact that Bombay chalcedony is distinct from the bulk of the samples in being a microcrystalline quartz may be related to this, however, Grape chalcedony also has a similar morphology and does not possess the population of very active sites.

The increased ice nucleation associated with milling may be caused by the mechanical fracturing of the quartz leading to exposure of high energy but unstable sites, which decay away through a structural rearrangement process when exposed to air or liquid water. Alternatively, milling may simply result in the removal of reaction products to leave exposed active sites. Kumar et al (2018) suggest the milling process causes the breakage of Si-O bonds which act as high energy sites for ice nucleation. Quartz does not exhibit a preferential plane of weakness (cleavage) to break along and it therefore fractures. The presence of small impurities distributed throughout the lattice, as described in sections 2 and 3, may influence the nature of fracturing and hence create differing defects and high energy sites. Gallagher (1987) classified impurities as a form of structural weakness. The impurities can create zones of weakness and stress within the crystal structure and therefore act as a pathway of least resistance resulting in the breakage of bonds and development of microtexture. Alternatively, in some instances the impurities may create areas of greater strength and so fracturing occurs around these zones. Hence, it is possible that the presence of impurities influences the way in which individual quartz samples fracture and therefore influence the presence of active sites.

Inherently, quartz is rather simple in terms of naturally occurring defects compared to other minerals, such as feldspar. In fact, in the past quartz has been considered to be in the 'perfect crystal class', i.e. lacking imperfections. However, quartz does have defects, albeit at a lower density than other materials (Spencer and Smith (1966)). Quartz minerals can be subject to varying conditions and stresses after their formation and so the geological history of the quartz may also influence the degree of microtexture. For example, a quartz sample which has undergone stress at a fault boundary is more likely to exhibit microtextural features than one that has not (Mahaney et al., 2004). It may be these microtextural differences that leads to the observed variability ice-nucleating ability between different quartz samples. This hypothesis might be tested in the future if quartz samples could be obtained with well characterised geological histories.

It has also been observed in the past that, for other minerals, the specifics of the mineral formation mechanism are critical for determining its ice-nucleating ability. Whale et al. (2017) demonstrated that a sample of K-feldspar, which had cooled sufficiently quickly during its formation that it did not undergo exsolution and therefore lacked the associated microtextures, had very poor ice nucleation properties. This was in contrast to the more common K-feldspars which do have exsolution microtexture and nucleate ice very effectively. Despite having very different ice-nucleating properties, their crystal structures and compositions are very similar. A similar formation pathway dependence may be true for quartz, such as strain introduced in geological fault systems. But one thing is clear: while bulk mineralogy is a guide to ice-nucleating activity, in some cases details of the formation pathway may be more important.

5 The importance of quartz relative to feldspar for ice nucleation in the atmosphere

5.1 Comparison to the literature data for quartz and feldspar

The data from the present study are contrasted with literature active site density data for quartz (Atkinson et al., 2013; Zolles et al., 2015) in Fig. 4. This data is also compared with $n_s(T)$ parameterisations for desert dust samples (Niemand et al., 2012; Ullrich et al., 2017) and K-feldspar (Atkinson et al., 2013). The variability within the α-quartz samples that we report is also reflected in the literature data for quartz. It is striking that two of the quartz samples in this study, Bombay chalcedony and Atkinson quartz, have an activity approaching or equal to K-feldspar. Nevertheless, it is apparent that quartz is never substantially more active than K-feldspar or desert dust in terms of $n_s(T)$.

Since one of our objectives is to determine how effective quartz is at nucleating ice in comparison to feldspars, we contrast the literature active site density data for feldspars and quartz in Fig. 5. The feldspars have been colour coded into the plagioclase (blue), albite (green) and the K-feldspar (orange-reds) groups. We note that, by convention, albite is considered part of the plagioclase solid solution series. However, Harrison et al. (2016) demonstrated that albites had a distinct nucleating activity and therefore we plot them here as a separate group. The K-feldspars presented here represent the K-rich samples from the alkali feldspar group (i.e. >10 % K). Overall there is a general trend in that plagioclase feldspars are the least active of the four mineral groups and K-feldspar is the most active. Both albite and quartz show similar, intermediate, activities. K-feldspars from Whale et al. (2017) which did not exhibit the common phase separation were excluded from this plot as they are unrepresentative of common K-feldspars and are rare in nature. Although quartz is an ice active material, Fig. 5 supports the consensus that it is the K-feldspars that are the most active mineral for ice nucleation that is commonly found in mineral dusts in the atmosphere.

5.2 New parameterisations for the ice-nucleating activity of quartz, K-feldspar, plagioclase and albite

In order to be able to determine which mineral is most important in the atmosphere we need the activity of each mineral (expressed as $n_s(T)$) in combination with estimates of the abundance of each mineral in the atmosphere. In this section we produce new $n_s(T)$ parameterisations for quartz, K-feldspar, plagioclase and albite using data from the present study in addition to literature data.

The new set of parameterisations are shown in Fig. 6. In order to derive these parameterisations we compiled data for representative samples of quartz, K-feldspar, plagioclase and albite. To create these parameterisations we binned the data within each dataset into 1 °C intervals and then fitted a polynomial line through the log averages of the data. We binned the data in an attempt to remove bias towards datasets with relatively high data density. In addition, we only applied a fit in the temperature range where multiple datasets were present (with the exception of plagioclase, where the available data is so sparse in some temperature regimes that we had to relax this criterion in order to produce a parameterisation). We used polynomial fits to represent the data since the data is quite complex and alternatives such as a straight line would produce a very poor representation of the data. However, when unconstrained the polynomial fits poorly represented the data at the warmest and coldest ends, hence we constrained the fits. We stress that these fits must not be extrapolated to higher and lower temperatures. The standard deviation for each parameterisation was calculated by taking the average of the standard deviations of the log $n_s(T)$ values for each 1 °C temperature interval. The corresponding value was then used to approximate the standard deviation from each fit, which is represented by the dashed lines and shaded area in Fig. 6.

For the quartz fit, the chalcedony samples were excluded given these microcrystalline materials are unrepresentative of most quartz in nature and that they are therefore likely to be in negligible abundances in the atmosphere. We also only include the runs with freshly made quartz suspensions in the parameterisation since the

second runs often showed signs of deactivation in suspension. By only using the relatively fresh suspension data, our parameterisation is representative of fresh, minimally-aged quartz dust. The new parameterisation can be seen in Fig. 6a-b and covers a temperature range of -12.5 °C to -37.5 °C and nine orders of magnitude in $n_s(T)$. This is the first robust $n_s(T)$ parameterisation developed for this mineral that can be used to determine its role as an INP in the atmosphere.

The K-feldspar parameterisation developed by Atkinson et al. (2013) has been used extensively within the ice nucleation community. However, this parameterisation was created with data from one K-feldspar sample and does not reflect the variability we now know to exist. The parameterisation developed as part of this study can be seen in Fig. 6c-d. We excluded K-feldspar samples which did not exhibit phase separation from the Whale et al. (2017) study from this parameterisation as these types of alkali feldspar are rare and unlikely to be found in significant quantities in the atmosphere. The strongly hyperactive TUD #3, examined by Harrison et al. (2016) and Peckhaus et al. (2016), was excluded as it exhibited extremely high activity and appears to be an exceptional case which is generally unrepresentative of the K-feldspar group of minerals. With this in mind we have developed a parameterisation which represents the bulk of the K-feldspars. It should be noted that all of the studies used BET derived surface areas for the calculation of $n_s(T)$ other than DeMott et al. (2018) and Augustin-Bauditz *et al.* (2014) who used geometric surface areas. However, while the difference between BET and geometric surface areas is substantial for clay samples (Hiranuma et al., 2015), the discrepancy is much smaller for materials with larger grain sizes like feldspar (Atkinson et al. 2013). When the new K-feldspar parameterisation is compared to the literature data it represents the variability of K-feldspar, as well as the curvature in the datasets. In particular, the new parameterisation captures the observed plateau in $n_s(T)$ below about -30 °C. In addition, the new parameterisation produces higher $n_s(T)$ values at temperatures warmer than -10 °C relative to that of Atkinson et al. (2013). Below -10 °C this new parameterisation gives lower values of $n_s(T)$. The temperature range of the parameterisation is also extended, covering -3.5 °C to -37.5 °C.

The parameterisation proposed here to represent plagioclase feldspar is shown in Fig. 6e-f. The parameterisation spans a temperature range of -12.5 °C to -38.5 °C. Only one dataset was available to represent the plagioclase feldspars in the lowest temperature regime (Zolles et al., 2015), hence this parameterisation needs to be used cautiously, but it is nonetheless a best estimate at present given the current data available. A similar caution must be accepted when using the albite parameterisation displayed in Fig. 6g-h which spans a range of -6.5 °C to -35.5 °C. For the albite parameterisation, the hyperactive Amelia albite from the Harrison et al. (2016) study was excluded due to it exhibiting exceptional behaviour and being unrepresentative of the other five albite samples. Hence, this parameterisation is representative of the non-hyperactive albites.

The parameterisations are summarised in Fig. 7a and are then combined with a typical abundance of each mineral to estimate the INP concentration ($[INP]_T$) associated with each of the four materials in Fig. 7b. On average, roughly 3±6 % (by mass) of atmospheric transported mineral dust particles are K-feldspar whereas 16±15 % are quartz and 8±3 % are plagioclase (see compilations of measurements in (Atkinson et al., 2013)). Albite is often grouped with plagioclase feldspars when determining the mineralogy of atmospheric mineral dusts rather than being reported on its own. For the purposes of this estimate we have assumed that albite has a concentration equal to 10 % of that of plagioclase. $[INP]_T$ was derived from the $n_s(T)$ parameterisations assuming a surface area concentration of mineral dust of 50 μm^2 cm^{-3} (a moderately dusty environment) and assuming that the mass fraction of each mineral is equivalent to its surface area fraction. In order to approximate the size distribution of dust, a lognormal size distribution centred around particles of 1 µm in diameter with a standard deviation of 0.3 was used. We have also assumed that each mineral is externally mixed (see Atkinson et al. (2013) for details of how to treat the mixing state of mineral dust), which is the assumption that has been made when modelling the global distribution of INP in the past (Atkinson et al., 2013 and Vergara-Temprado et al., 2017). In reality, desert dust aerosol will be somewhat internally mixed. The opposing assumption of full internal mixing produces 1-2 orders more INP at the lowest temperatures, but produces the same INP concentration above about -25°C (Atkinson et al. 2013). The upper and lower bounds for each line in Fig 7b are derived from the range of mineral mass concentrations.

The $[INP]_T$ curves in Fig. 7b confirm that under most atmospheric situations K-feldspar has the main contribution to the ice-nucleating particle population in desert dust. Quartz is the next most important mineral, with plagioclase the least important. The contribution of pure albite is rather uncertain given the amount of pure albite in desert dust is poorly constrained, but it is unlikely to compete with K-feldspar. Nevertheless, while K-feldspar is the most important contributor to the INP population, the estimates in Fig. 7b do suggest that quartz may make a non-

negligible contribution to the INP budget at temperatures between about -20 and -12.5 °C. This is particularly so when we consider the variability in the ice-nucleating ability of the K-feldspar and quartz groups. It is possible that in a desert dust aerosol that if the K-feldspar was at the bottom end of the activity, whereas the quartz were at the top end of its activity range, then the quartz would contribute more INP than K-feldspar. However, it should also be considered that the estimated $[INP]_T$ curves in Fig. 7b are also based on the assumption that quartz has the activity of fresh quartz. We know from the work presented above that the activity of quartz is sensitive to ageing processes. We cannot quantify ageing of atmospheric quartz, but the parameterisation we present here probably represents an upper limit to its activity. In contrast, the activity of K-feldspar does not decrease with time spent in water or air (Harrison et al., 2016; Whale et al., 2017). Overall, we conclude that K-feldspar contributes the bulk of the INPs associated with desert dust, because it is more active and it is less sensitive to ageing processes. However, we should not rule out quartz making a significant contribution to the INP population in a minority of cases.

5.3 Testing the new parameterisations against literature laboratory and field measurements of the ice-nucleating ability of desert dust

We now test the quartz and K-feldspar parameterisations to see if they are consistent with literature data of the ice-nucleating ability of desert dust (Fig. 8). In Fig 8a we contrast the predicted $n_s(T)$ values, based on the quartz and K-feldspar parameterisations, against a variety of literature datasets for desert dust. For the K-feldspar based prediction, we have presented lines where 20 %, 1 % and 0.1 % of the surface area of dust is made up of K-feldspar. For the 20 % prediction, which is consistent with measurements in Cape Verde (Kandler et al., 2011), we have also shown the natural variability in K-feldspar activity as the shaded region. The line assuming quartz is the dominant ice-nucleating mineral in desert dust is for 12 % quartz which again is consistent with measurements made in Cape Verde (Kandler et al., 2011).

From Fig. 8a it is clear that quartz does not account for the $n_s(T)$ measurements of desert dusts sampled directly from the atmosphere and suspended in laboratory studies. However, the new K-feldspar parameterisation is consistent with the ice-nucleating activity of dusts over a wide range of temperatures. The K-feldspar parameterisation reasonably represents the majority of mineral dust measurements when taking into account that typically ~1 % to 25 % of atmospheric desert dust can be attributed to K-feldspar (Atkinson et al., 2013) and that there is a natural variability in the ice-nucleating ability of K-feldspar (as presented by the shaded area around the 20 % K-feldspar prediction). The shape of the parameterisation represents the bulk of the data well and plateaus at the lowest temperatures in agreement with the observations.

Fig. 8b shows INP concentrations measured from an aircraft in the eastern tropical Atlantic (Price et al., 2018) plotted with the predicted INP concentrations based on the K-feldspar parameterisation developed by Atkinson et al. (2013) (in black dashed lines), the parameterisation for desert dust by Niemand et al. (2012) (orange dashed lines) and the K-feldspar parameterisation proposed here (red dashed lines). The parameterisations were calculated assuming an externally mixed scenario (although both internal and external mixing assumptions produce a similar result in the regime where the measurements were made). The upper and lower bounds were calculated by incorporating the maximum and minimum in the aerosol surface area concentrations corresponding to the various aircraft measurements (23.8 $\mu m^2\ cm^{-3}$ to 1874 $\mu m^2\ cm^{-3}$) (Price et al, 2018). K-feldspar was assumed to represent 20 % of the aerosol surface area, based on measurements by Kandler et al. (2011). Note that the small number of data points above ~-11°C have a very high uncertainty due to Poisson counting issues and should be regarded as upper limits. Price et al. (2018) and Sanchez-Marroquin et al. (*in preparation*) have described a sub-isokinetic sampling bias in the aircraft inlet which results in an enhancement of aerosol surface area by roughly a factor of 2.5 for the used sampling conditions. We have therefore corrected the Price et al. (2018) data downwards by a factor of 2.5 (although on the log scale this makes a relatively small difference).

We can see that the Atkinson et al. (2013) parameterisation is a relatively poor predictor of the INP concentration, especially at temperatures colder than about -15 °C. The parameterisation by Niemand et al. (2012) tends to over-predict INP concentrations relative to the Price et al. (2018) data by about one order of magnitude. However, the K-feldspar parameterisation proposed here better represents the magnitude, the range and the slope of the aircraft data. Overall, the new K-feldspar parameterisation provides a good representation of the ice-nucleating activity of dust from field and laboratory studies and it is also clear that quartz is of second order importance for desert dust's ice-nucleating ability.

2 Conclusions

We have studied 10 quartz samples for their ice-nucleating ability in order to better understand and define the ice-activity of this abundant mineral. The chosen samples were all α-quartz, the most common silica polymorph found at the Earth's surface, but included a variety of α-quartz types with varying degrees of impurities and different crystal habits. We found that the ice-nucleating activity of these samples is surprisingly variable, spanning about 10 °C. Eight out of ten of the quartz samples lay within -17 °C to -20 °C at $n_s(T) = 10$ cm^{-2}, with two quartz samples, Bombay chalcedony and Atkinson quartz, being much more active (as active as K-feldspar). Overall, the quartz group of minerals tend to be less active than the K-feldspars, slightly less active than albite, but more active than the plagioclase feldspars. In the future it would be interesting to probe the nature of the active sites on the two most active samples and to try to contrast these sites to those on the less active samples in order to further understand the nature of active sites and why they have such strongly contrasting characteristics.

Although quartz is regarded as a relatively chemically inert mineral the activity of some samples decreases with time spent in air and water. Most of the samples were sensitive to time spent in water, but interestingly, the most active sample's activity did not change significantly even after many months in water. We note that the sensitivity to time in water displayed by most of the quartz samples studied here is in strong contrast to K-feldspars, which tend to be much more stable. We suggest that further work be focused on the impact of 'weathering' processes, not just on quartz, but all atmospherically relevant mineral INPs. Related to this, we also note that solutes can alter the ice nucleating ability of mineral samples (Whale et al., 2018). The sensitivity to these ageing processes could be very important in determining the dominant INP types globally and may also offer a window into an improved fundamental understanding of ice nucleation by minerals in general.

To investigate the relative importance of quartz to feldspars in the atmosphere we have proposed new active site density parameterisations for quartz, K-feldspar, plagioclase and albite. These parameterisations are based on a combination of the data presented here for quartz along with data available in the literature. When using the newly developed parameterisations to predict INP concentrations in combination with typical atmospheric abundances of minerals, it is found that K-feldspar typically produces more INP than quartz (or any other mineral). In addition, we find that the newly developed K-feldspar parameterisation is consistent with $n_s(T)$ literature measurements on desert dusts and better represents field measurements of INP concentrations in the dusty tropical Atlantic compared to the parameterisations by Atkinson et al. (2013) and Niemand et al. (2012). We hereby propose the use of this new parameterisation when predicting INP concentrations related to mineral dusts.

Author contributions: ADH designed the experiments with help from scientific discussions with BJM, TFW and JBM. Both KL and ADH performed the experiments. AS completed the calculations for the external mixing assumption used in figures 7b and 8a and assisted in the calculation of errors for the active site density measurements. MAH carried out Raman analysis of the chalcedony samples and MDT helped in the assembly of the literature data. ADH prepared the manuscript with contributions from all co-authors.

7 References

Ansmann, A., Tesche, M., Seifert, P., Althausen, D., Engelmann, R., Fruntke, J., Wandinger, U., Mattis, I., and Müller, D.: Evolution of the ice phase in tropical altocumulus: SAMUM lidar observations over Cape Verde, Journal of Geophysical Research: Atmospheres, 114, D17208, 2009.

Applin, K. R. and Hicks, B. D.: Fibers of dumortierite in quartz, American Mineralogist, 72, 170-172, 1987.

Atkinson, J. D., Murray, B. J., Woodhouse, M. T., Whale, T. F., Baustian, K. J., Carslaw, K. S., Dobbie, S., O'Sullivan, D., and Malkin, T. L.: The importance of feldspar for ice nucleation by mineral dust in mixed-phase clouds, Nature, 498, 355-358, 2013.

Avila, A., Queralt-Mitjans, I., and Alarcón, M.: Mineralogical composition of African dust delivered by red rains over northeastern Spain, Journal of Geophysical Research: Atmospheres, 102, 21977-21996, 1997.

Boose, Y., Sierau, B., Garcia, I. M., Rodriguez, S., Alastuey, A., Linke, C., Schnaiter, M., Kupiszewski, P., Kanji, Z. A., and Lohmann, U.: Ice nucleating particles in the Saharan Air Layer, Atmos. Chem. and Phys., 16, 9067-9087, 2016a.

Boose, Y., Welti, A., Atkinson, J., Ramelli, F., Danielczok, A., Bingemer, H. G., Plötze, M., Sierau, B., Kanji, Z. A., and Lohmann, U.: Heterogeneous ice nucleation on dust particles sourced from nine deserts worldwide – Part 1: Immersion freezing, Atmospheric Chemistry and Physics, 16, 15075-15095, 2016b.

543 Broadley, S. L., Murray, B. J., Herbert, R. J., Atkinson, J. D., Dobbie, S., Malkin, T. L., Condliffe, E., and Neve,
544 L.: Immersion mode heterogeneous ice nucleation by an illite rich powder representative of atmospheric mineral
545 dust, Atmos. Chem. Phys., 12, 287-307, 2012.
546 Caquineau, S., Gaudichet, A., Gomes, L., Magonthier, M.-C., and Chatenet, B.: Saharan dust: Clay ratio as a
547 relevant tracer to assess the origin of soil-derived aerosols, Geophysical Research Letters, 25, 983-986, 1998.
548 Connolly, P. J., Möhler, O., Field, P. R., Saathoff, H., Burgess, R., Choularton, T., and Gallagher, M.: Studies of
549 heterogeneous freezing by three different desert dust samples, Atmos. Chem. Phys., 9, 2805-2824, 2009.
550 Deer, W. A., Howie, R. A., and Zussman, J.: An introduction to the rock forming minerals, Addison Wesley
551 Longman, Harlow, UK, 1992.
552 Deer, W. A., Howie, R. A., and Zussman, J.: An introduction to thr rock forming minerals, Longman group
553 limited, London, 1966.
554 DeMott, P. J., Möhler, O., Cziczo, D. J., Hiranuma, N., Petters, M. D., Petters, S. S., Belosi, F., Bingemer, H. G.,
555 Brooks, S. D., Budke, C., Burkert-Kohn, M., Collier, K. N., Danielczok, A., Eppers, O., Felgitsch, L., Garimella,
556 S., Grothe, H., Herenz, P., Hill, T. C. J., Höhler, K., Kanji, Z. A., Kiselev, A., Koop, T., Kristensen, T. B., Krüger,
557 K., Kulkarni, G., Levin, E. J. T., Murray, B. J., Nicosia, A., amp, apos, Sullivan, D., Peckhaus, A., Polen, M. J.,
558 Price, H. C., Reicher, N., Rothenberg, D. A., Rudich, Y., Santachiara, G., Schiebel, T., Schrod, J., Seifried, T. M.,
559 Stratmann, F., Sullivan, R. C., Suski, K. J., Szakáll, M., Taylor, H. P., Ullrich, R., Vergara-Temprado, J., Wagner,
560 R., Whale, T. F., Weber, D., Welti, A., Wilson, T. W., Wolf, M. J., and Zenker, J.: The Fifth International
561 Workshop on Ice Nucleation phase 2 (FIN-02): laboratory intercomparison of ice nucleation measurements,
562 Atmospheric Measurement Techniques, 11, 6231-6257, 2018.
563 DeMott, P. J., Möhler, O., Stetzer, O., Vali, G., Levin, Z., Petters, M. D., Murakami, M., Leisner, T., Bundke, U.,
564 Klein, H., Kanji, Z. A., Cotton, R., Jones, H., Benz, S., Brinkmann, M., Rzesanke, D., Saathoff, H., Nicolet, M.,
565 Saito, A., Nillius, B., Bingemer, H., Abbatt, J., Ardon, K., Ganor, E., Georgakopoulos, D. G., and Saunders, C.:
566 Resurgence in Ice Nuclei Measurement Research, Bulletin of the American Meteorological Society, 92, 1623-
567 1635, 2011.
568 DeMott, P. J., Prenni, A. J., McMeeking, G. R., Sullivan, R. C., Petters, M. D., Tobo, Y., Niemand, M., Möhler,
569 O., Snider, J. R., Wang, Z., and Kreidenweis, S. M.: Integrating laboratory and field data to quantify the immersion
570 freezing ice nucleation activity of mineral dust particles, Atmospheric Chemistry and Physics, 15, 393-409, 2015.
571 Eriksen Hammer, S., Mertes, S., Schneider, J., Ebert, M., Kandler, K., and Weinbruch, S.: Composition of ice
572 particle residuals in mixed phase clouds at Jungfraujoch (Switzerland): Enrichment and depletion of particle
573 groups relative to total aerosol, Atmospheric Chemistry and Physics Discussions, doi: 10.5194/acp-2018-478,
574 2018. 1-27, 2018.
575 Field, P. R., Lawson, R. P., Brown, P. R. A., Lloyd, G., Westbrook, C., Moisseev, D., Miltenberger, A., Nenes,
576 A., Blyth, A., Choularton, T., Connolly, P., Buehl, J., Crosier, J., Cui, Z., Dearden, C., DeMott, P., Flossmann,
577 A., Heymsfield, A., Huang, Y., Kalesse, H., Kanji, Z. A., Korolev, A., Kirchgaessner, A., Lasher-Trapp, S.,
578 Leisner, T., McFarquhar, G., Phillips, V., Stith, J., and Sullivan, S.: Chapter 7. Secondary Ice Production - current
579 state of the science and recommendations for the future, Meteorological Monographs, doi:
580 10.1175/amsmonographs-d-16-0014.1, 2016. 2016.
581 Gallagher, J. J.: Fractography of sand grains broken by uniaxial compression, Van Nostrand Reinhold, New York,
582 USA, 1987.
583 Glaccum, R. A. and Prospero, J. M.: Saharan aerosols over the tropical North Atlantic — Mineralogy, Marine
584 Geology, 37, 295-321, 1980.
585 Goreva, J. S., Ma, C., and Rossman, G. R.: Fibrous nanoinclusions in massive rose quartz: The origin of rose
586 coloration, American Mineralogist, 86, 466-472, 2001.
587 Götze, J., Nasdala, L., Kleeberg, R., and Wenzel, M.: Occurrence and distribution of "moganite" in
588 agate/chalcedony: a combined micro-Raman, Rietvel and cathodoluminescence study, Contributions to
589 Mineralogy and Petrology, 133, 96-105, 1998.
590 Harrison, A. D., Whale, T. F., Carpenter, M. A., Holden, M. A., Neve, L., apos, Sullivan, D., Vergara Temprado,
591 J., and Murray, B. J.: Not all feldspars are equal: a survey of ice nucleating properties across the feldspar group
592 of minerals, Atmospheric Chemistry and Physics, 16, 10927-10940, 2016.
593 Heaney, P. J. and Post, J. E.: The widespread distribution of a novel silica polymorph in microcrystalline quartz
594 varieties, Science, 255, 441-443, 1992.
595 Herbert, R. J., Murray, B. J., Dobbie, S. J., and Koop, T.: Sensitivity of liquid clouds to homogenous freezing
596 parameterizations, Geophysical Research Letters, 42, 1599-1605, 2015.
597 Herbert, R. J., Murray, B. J., Whale, T. F., Dobbie, S. J., and Atkinson, J. D.: Representing time-dependent
598 freezing behaviour in immersion mode ice nucleation, Atmospheric Chemistry and Physics, 14, 8501-8520, 2014.
599 Hiranuma, N., Augustin-Bauditz, S., Bingemer, H., Budke, C., Curtius, J., Danielczok, A., Diehl, K.,
600 Dreischmeier, K., Ebert, M., Frank, F., Hoffmann, N., Kandler, K., Kiselev, A., Koop, T., Leisner, T., Möhler,
601 O., Nillius, B., Peckhaus, A., Rose, D., Weinbruch, S., Wex, H., Boose, Y., DeMott, P. J., Hader, J. D., Hill, T.
602 C. J., Kanji, Z. A., Kulkarni, G., Levin, E. J. T., McCluskey, C. S., Murakami, M., Murray, B. J., Niedermeier,

603 D., Petters, M. D., O'Sullivan, D., Saito, A., Schill, G. P., Tajiri, T., Tolbert, M. A., Welti, A., Whale, T. F.,
604 Wright, T. P., and Yamashita, K.: A comprehensive laboratory study on the immersion freezing behavior of illite
605 NX particles: a comparison of 17 ice nucleation measurement techniques, Atmos. Chem. Phys., 15, 2489-2518,
606 2015.
607 Holden, M. A., Whale, T. F., Tarn, M. D., O'Sullivan, D., Walshaw, R. D., Murray, B. J., Meldrum, F. C., and
608 Christenson, H. K.: High-speed imaging of ice nucleation in water proves the existence of active sites, Sci. Adv.,
609 2019. 2019.
610 Hoose, C. and Möhler, O.: Heterogeneous ice nucleation on atmospheric aerosols: a review of results from
611 laboratory experiments, Atmos. Chem. Phys., 12, 9817-9854, 2012.
612 Isono, K. and Ikebe, Y.: On the Ice-nucleating Ability of Rock-forming Minerals and Soil Particles&lowast,
613 Journal of the Meteorological Society of Japan. Ser. II, 38, 213-230, 1960.
614 Iwata, A. and Matsuki, A.: Characterization of individual ice residual particles by the single droplet freezing
615 method: a case study in the Asian dust outflow region, Atmospheric Chemistry and Physics, 18, 1785-1804, 2018.
616 James, A. D., Brooke, J. S. A., Mangan, T. P., Whale, T. F., Plane, J. M. C., and Murray, B. J.: Nucleation of
617 nitric acid hydrates in polar stratospheric clouds by meteoric material, Atmospheric Chemistry and Physics, 18,
618 4519-4531, 2018.
619 Kandler, K., Schütz, L., Deutscher, C., Ebert, M., Hofmann, H., Jäckel, S., Jaenicke, R., Knippertz, P., Lieke, K.,
620 Massling, A., Petzold, A., Schladitz, A., Weinzierl, B., Wiedensohler, A., Zorn, S., and Weinbruch, S.: Size
621 distribution, mass concentration, chemical and mineralogical composition and derived optical parameters of the
622 boundary layer aerosol at Tinfou, Morocco, during SAMUM 2006, Tellus, 61B, 32-50, 2009.
623 Kandler, K., SchÜTz, L., JÄCkel, S., Lieke, K., Emmel, C., MÜLler-Ebert, D., Ebert, M., Scheuvens, D.,
624 Schladitz, A., ŠEgviĆ, B., Wiedensohler, A., and Weinbruch, S.: Ground-based off-line aerosol measurements at
625 Praia, Cape Verde, during the Saharan Mineral Dust Experiment: microphysical properties and mineralogy,
626 Tellus, 63B, 459-474, 2011.
627 Kanitz, T., Seifert, P., Ansmann, A., Engelmann, R., Althausen, D., Casiccia, C., and Rohwer, E. G.: Contrasting
628 the impact of aerosols at northern and southern midlatitudes on heterogeneous ice formation, Geophys. Res. Lett.,
629 38, L17802, 2011.
630 Kanji, Z. A., DeMott, P. J., Möhler, O., and Abbatt, J. P. D.: Results from the University of Toronto continuous
631 flow diffusion chamber at ICIS 2007: instrument intercomparison and ice onsets for different aerosol types,
632 Atmospheric Chemistry and Physics, 11, 31-41, 2011.
633 Kanji, Z. A., Ladino, L. A., Wex, H., Boose, Y., Burkert-Kohn, M., Cziczo, D. J., and Krämer, M.: Overview of
634 Ice Nucleating Particles, Meteorological Monographs, 58, 1.1-1.33, 2017.
635 Kibar, R., Garcia-Guinea, J., Çetin, A., Selvi, S., Karal, T., and Can, N.: Luminescent, optical and color properties
636 of natural rose quartz, Radiation Measurements, 42, 1610-1617, 2007.
637 Koehler, K. A., Kreidenweis, S. M., DeMott, P. J., Petters, M. D., Prenni, A. J., and Möhler, O.: Laboratory
638 investigations of the impact of mineral dust aerosol on cold cloud formation, Atmospheric Chemistry and Physics,
639 10, 11955-11968, 2010.
640 Koike, C., Noguchi, R., Chihara, H., Suto, H., Ohtaka, O., Imai, Y., Matsumoto, T., and Tsuchiyama, A.: Infrared
641 Spectra of Silica Polymorphs and the Conditions of Their Formation, The Astrophysical Journal, 778, 60, 2013.
642 Kumar, A., Marcolli, C., and Peter, T.: Ice nucleation activity of silicates and aluminosilicates in pure water and
643 aqueous solutions. Part 2 - Quartz and amorphous silica, Atmospheric Chemistry and Physics Discussions, doi:
644 10.5194/acp-2018-1020, 2018. 1-35, 2018.
645 Lohmann, U.: Anthropogenic Aerosol Influences on Mixed-Phase Clouds, Current Climate Change Reports, 3,
646 32-44, 2017.
647 Mahaney, W. C., Dirszowsky, R. W., Milner, M. W., Menzies, J., Stewart, A., Kalm, V., and Bezada, M.: Quartz
648 microtextures and microstructures owing to deformation of glaciolacustrine sediments in the northern Venezuelan
649 Andes, Journal of Quaternary Science, 19, 23-33, 2004.
650 Mason, B. J. and Maybank, J.: ICE-NUCLEATING PROPERTIES OF SOME NATURAL MINERAL DUSTS,
651 Quarterly Journal of the Royal Meteorological Society, 84, 235-241, 1958.
652 Murray, B. J., Broadley, S. L., Wilson, T. W., Atkinson, J. D., and Wills, R. H.: Heterogeneous freezing of water
653 droplets containing kaolinite particles, Atmospheric Chemistry and Physics, 11, 4191-4207, 2011.
654 Murray, B. J., O'Sullivan, D., Atkinson, J. D., and Webb, M. E.: Ice nucleation by particles immersed in
655 supercooled cloud droplets, Chemical Society Reviews, 41, 6519-6554, 2012.
656 Nassau, K.: The origins of color in minerals, American Mineralogist, 63, 219-229, 1978.
657 Niedermeier, D., Augustin-Bauditz, S., Hartmann, S., Wex, H., Ignatius, K., and Stratmann, F.: Can we define an
658 asymptotic value for the ice active surface site density for heterogeneous ice nucleation?, Journal of Geophysical
659 Research: Atmospheres, 120, 5036-5046, 2015.
660 Niemand, M., Möhler, O., Vogel, B., Vogel, H., Hoose, C., Connolly, P., Klein, H., Bingemer, H., DeMott, P. J.,
661 Skrotzki, J., and Leisner, T.: A particle-surface-area-based parameterization of immersion freezing on desert dust
662 particles, Journal of the Atmospheric Sciences, 69, 2012.

O'Sullivan, D., Murray, B. J., Malkin, T. L., Whale, T. F., Umo, N. S., Atkinson, J. D., Price, H. C., Baustian, K. J., Browse, J., and Webb, M. E.: Ice nucleation by fertile soil dusts: relative importance of mineral and biogenic components, Atmos. Chem. Phys., 14, 1853-1867, 2014.

Peckhaus, A., Kiselev, A., Hiron, T., Ebert, M., and Leisner, T.: A comparative study of K-rich and Na/Ca-rich feldspar ice nucleating particles in a nanoliter droplet freezing assay, Atmos. Chem. Phys. Discuss., 2016, 1-43, 2016.

Pedevilla, P., Fitzner, M., and Michaelides, A.: What makes a good descriptor for heterogeneous ice nucleation on OH-patterned surfaces, Physical Review B, 96, 2017.

Perlwitz, J. P., Pérez García-Pando, C., and Miller, R. L.: Predicting the mineral composition of dust aerosols – Part 1: Representing key processes, Atmos. Chem. Phys., 15, 11593-11627, 2015.

Pinti, V., Marcolli, C., Zobrist, B., Hoyle, C. R., and Peter, T.: Ice nucleation efficiency of clay minerals in the immersion mode, Atmos. Chem. Phys. Discuss., 12, 3213-3261, 2012.

Pratt, K. A., DeMott, P. J., French, J. R., Wang, Z., Westphal, D. L., Heymsfield, A. J., Twohy, C. H., Prenni, A. J., and Prather, K. A.: In situ detection of biological particles in cloud ice-crystals, Nature Geosci, 2, 398-401, 2009.

Price, H. C., Baustian, K. J., McQuaid, J. B., Blyth, A., Bower, K. N., Choularton, T., Cotton, R. J., Cui, Z., Field, P. R., Gallagher, M., Hawker, R., Merrington, A., Miltenberger, A., Neely Iii, R. R., Parker, S. T., Rosenberg, P. D., Taylor, J. W., Trembath, J., Vergara-Temprado, J., Whale, T. F., Wilson, T. W., Young, G., and Murray, B. J.: Atmospheric Ice-Nucleating Particles in the Dusty Tropical Atlantic, Journal of Geophysical Research: Atmospheres, 123, 2175-2193, 2018.

Pummer, B. G., Budke, C., Augustin-Bauditz, S., Niedermeier, D., Felgitsch, L., Kampf, C. J., Huber, R. G., Liedl, K. R., Loerting, T., Moschen, T., Schauperl, M., Tollinger, M., Morris, C. E., Wex, H., Grothe, H., Pöschl, U., Koop, T., and Fröhlich-Nowoisky, J.: Ice nucleation by water-soluble macromolecules, Atmos. Chem. Phys., 15, 4077-4091, 2015.

Reicher, N., Segev, L., and Rudich, Y.: The WeIzmann Supercooled Droplets Observation on a Microarray (WISDOM) and application for ambient dust, Atmospheric Measurement Techniques, 11, 233-248, 2018.

Roberts, P. and Hallett, J.: A laboratory study of the ice nucleating properties of some mineral particulates, Quarterly Journal of the Royal Meteorological Society, 94, 25-34, 1968.

Rosenfeld, D., Yu, X., Liu, G., Xu, X., Zhu, Y., Yue, Z., Dai, J., Dong, Z., Dong, Y., and Peng, Y.: Glaciation temperatures of convective clouds ingesting desert dust, air pollution and smoke from forest fires, Geophysical Research Letters, 38, n/a-n/a, 2011.

Spencer, W. J. and Smith, W. L.: Defects in Natural Quartz, Journal of Applied Physics, 37, 2557-2563, 1966.

Swamy, V., Saxena, S. K., Sundman, B., and Zhang, J.: A thermodynamic assessment of silica phase diagram, Journal of Geophysical Research: Solid Earth, 99, 11787-11794, 1994.

Tan, I., Storelvmo, T., and Zelinka, M. D.: Observational constraints on mixed-phase clouds imply higher climate sensitivity, Science, 352, 224-227, 2016.

Tarn, M. D., Sikora, S. N. F., Porter, G. C. E., O'Sullivan, D., Adams, M., Whale, T. F., Harrison, A. D., Vergara-Temprado, J., Wilson, T. W., Shim, J. U., and Murray, B. J.: The study of atmospheric ice-nucleating particles via microfluidically generated droplets, Microfluid Nanofluidics, 22, 52, 2018.

Ullrich, R., Hoose, C., Möhler, O., Niemand, M., Wagner, R., Höhler, K., Hiranuma, N., Saathoff, H., and Leisner, T.: A New Ice Nucleation Active Site Parameterization for Desert Dust and Soot, Journal of the Atmospheric Sciences, 74, 699-717, 2017.

Umo, N. S., Murray, B. J., Baeza-Romero, M. T., Jones, J. M., Lea-Langton, A. R., Malkin, T. L., O'Sullivan, D., Neve, L., Plane, J. M. C., and Williams, A.: Ice nucleation by combustion ash particles at conditions relevant to mixed-phase clouds, Atmos. Chem. Phys., 15, 5195-5210, 2015.

Vali, G., DeMott, P. J., Möhler, O., and Whale, T. F.: Technical Note: A proposal for ice nucleation terminology, Atmospheric Chemistry and Physics, 15, 10263-10270, 2015.

Vergara-Temprado, J., Miltenberger, A. K., Furtado, K., Grosvenor, D. P., Shipway, B. J., Hill, A. A., Wilkinson, J. M., Field, P. R., Murray, B. J., and Carslaw, K. S.: Strong control of Southern Ocean cloud reflectivity by ice-nucleating particles, Proceedings of the National Academy of Sciences of the United States of America, 115, 2687-2692, 2018.

Vergara-Temprado, J., Murray, B. J., Wilson, T. W., amp, apos, Sullivan, D., Browse, J., Pringle, K. J., Ardon-Dryer, K., Bertram, A. K., Burrows, S. M., Ceburnis, D., DeMott, P. J., Mason, R. H., amp, apos, Dowd, C. D., Rinaldi, M., and Carslaw, K. S.: Contribution of feldspar and marine organic aerosols to global ice nucleating particle concentrations, Atmos. Chem. Phys., 17, 3637-3658, 2017.

Wex, H., DeMott, P. J., Tobo, Y., Hartmann, S., Rösch, M., Clauss, T., Tomsche, L., Niedermeier, D., and Stratmann, F.: Kaolinite particles as ice nuclei: learning from the use of different kaolinite samples and different coatings, Atmos. Chem. Phys., 14, 5529-5546, 2014.

721 Whale, T. F., Holden, M. A., Kulak, A. N., Kim, Y. Y., Meldrum, F. C., Christenson, H. K., and Murray, B. J.:
722 The role of phase separation and related topography in the exceptional ice-nucleating ability of alkali feldspars,
723 Phys Chem Chem Phys, 19, 31186-31193, 2017.
724 Whale, T. F., Holden, M. A., Wilson, T. W., O'Sullivan, D., and Murray, B. J.: The enhancement and suppression
725 of immersion mode heterogeneous ice-nucleation by solutes, Chem Sci, 9, 4142-4151, 2018.
726 Whale, T. F., Murray, B. J., O'Sullivan, D., Wilson, T. W., Umo, N. S., Baustian, K. J., Atkinson, J. D., Workneh,
727 D. A., and Morris, G. J.: A technique for quantifying heterogeneous ice nucleation in microlitre supercooled water
728 droplets, Atmos. Meas. Tech., 8, 2437-2447, 2015.
729 Wright, T. P., Petters, M. D., Hader, J. D., Morton, T., and Holder, A. L.: Minimal cooling rate dependence of ice
730 nuclei activity in the immersion mode, Journal of Geophysical Research-Atmospheres, 118, 10535-10543, 2013.
731 Zolles, T., Burkart, J., Häusler, T., Pummer, B., Hitzenberger, R., and Grothe, H.: Identification of Ice Nucleation
732 Active Sites on Feldspar Dust Particles, The Journal of Physical Chemistry A, 119, 2692-2700, 2015.

733

734

735

736

737

738

739

740

Sample	*XRD analysis*	*BET surface area (m^2g^{-1})*
Bombay chalcedony	α -quartz: 100%	1.23 ± 0.01
Grape chalcedony	α -quartz: 100%	4.39 ± 0.01
Smoky quartz	α -quartz: 98.3% Haematite: 0.1% Albite: 1.6%	1.23 ± 0.01
Rose quartz	α -quartz: 100%	1.13 ± 0.01
Atkinson quartz	α -quartz: 99.9% Calcite: 0.1%	4.20 ± 0.01
Fluka quartz	α -quartz: 100%	0.91 ± 0.01
Mexico quartz	α -quartz: 96.4% Dolomite: 3.6%	1.74 ± 0.01
LD1 quartz	α -quartz: 100%	0.94 ± 0.01
Uruguay amethyst	α -quartz: 99.9% Calcite: 0.1%	1.46 ± 0.01
Brazil amethyst	α -quartz: 100%	2.76 ± 0.01

741 **Table 1:** Table showing the relative concentrations of different minerals within each sample and the respective BET
742 derived surface area of the ground sample. The uncertainty in the XRD analysis is on the order of 0.1 %, hence the
743 identification of some trace constituents in some samples is tentative.

744

Atmos. Chem. Phys. Discuss., https://doi.org/10.5194/acp-2019-288
Manuscript under review for journal Atmos. Chem. Phys.
Discussion started: 12 April 2019

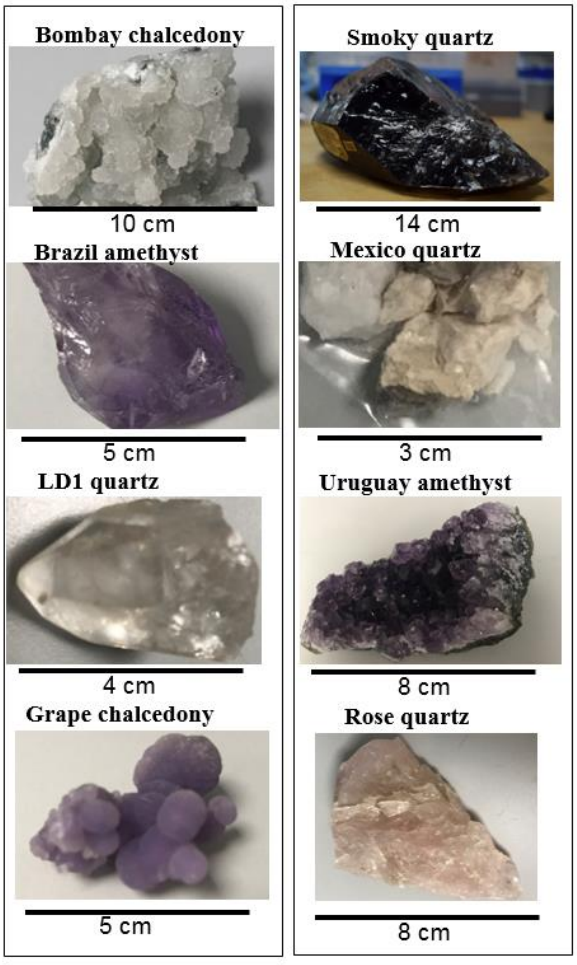

Figure 1: Pictures of the various quartz samples explored in this study showing their varying appearances and characteristics. Samples supplied in a ground state are not shown.

Atmos. Chem. Phys. Discuss., https://doi.org/10.5194/acp-2019-288
Manuscript under review for journal Atmos. Chem. Phys.
Discussion started: 12 April 2019

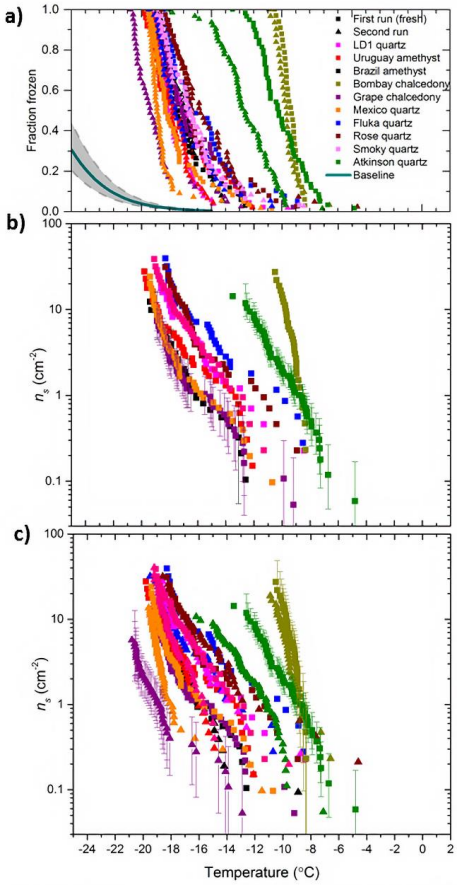

Figure 2: Fraction frozen and active site densities for 10 quartz samples. **a)** The fraction frozen versus temperature for the different quartz samples investigated in this study. The range of freezing for the baseline is highlighted in the grey shaded region (Umo et al., 2015). **(b)** The active site density ($n_s(T)$) for the range of quartz samples in this study. In this plot only the first run of each sample is displayed. These samples are considered to be fresh as they have only spent roughly 10 minutes in suspension. **(c)** The active site density ($n_s(T)$) versus temperature for the quartz samples on their initial runs and their corresponding second runs. The second runs were carried out roughly an hour after the first run. A sample of the error bars are shown in Fig. 2b/c.

Atmos. Chem. Phys. Discuss., https://doi.org/10.5194/acp-2019-288
Manuscript under review for journal Atmos. Chem. Phys.
Discussion started: 12 April 2019

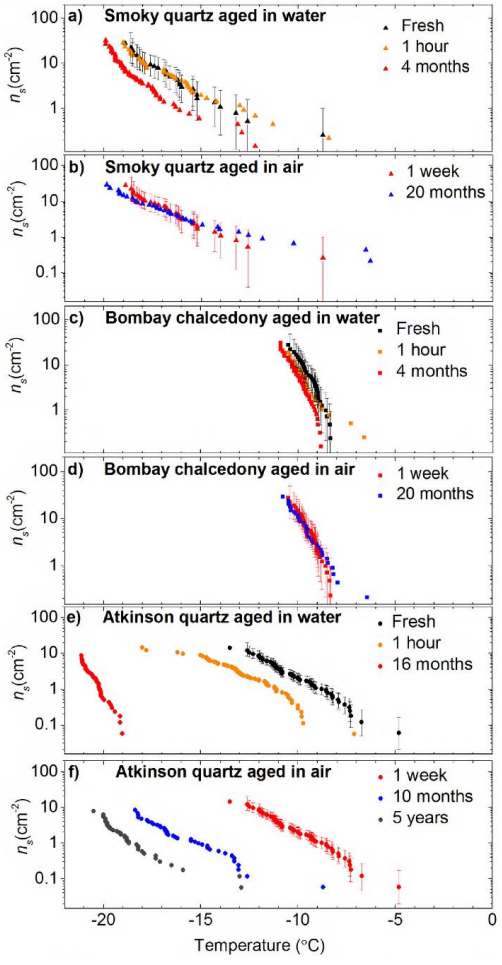

Figure 3: Plots showing the sensitivity of quartz activity, expressed as $n_s(T)$, to time spent in water and air. Data are shown for **(a and b)** Smoky quartz, **(c and d)** Bombay chalcedony and **(e and f)** Atkinson quartz. A sample of the error bars associated with each experiment are shown. The $n_s(T)$ values for the fresh (~10 min) and one hour suspensions were taken from Fig. 2.

Atmos. Chem. Phys. Discuss., https://doi.org/10.5194/acp-2019-288
Manuscript under review for journal Atmos. Chem. Phys.
Discussion started: 12 April 2019

Atmospheric Chemistry and Physics Discussions

776

777

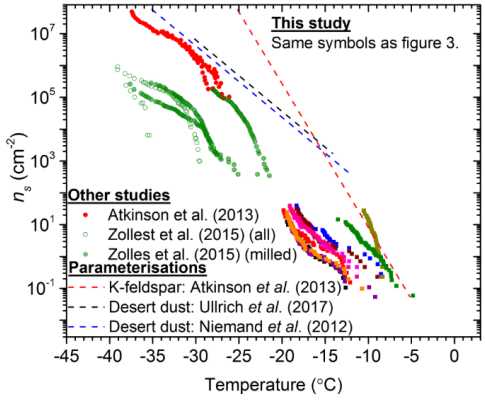

778

779 **Figure 4:** Plot of $n_s(T)$ versus temperature for the available literature data for quartz compared to the data collected in this
780 study. The symbols for this study's data are displayed the same as in Fig. 2 and only the first runs (fresh samples) from this
781 study are plotted. The data from Zolles et al. (2015) has been split into quartz samples which were milled for fresh surfaces
782 and all the combined data (both milled and un-milled quartz).

783

784

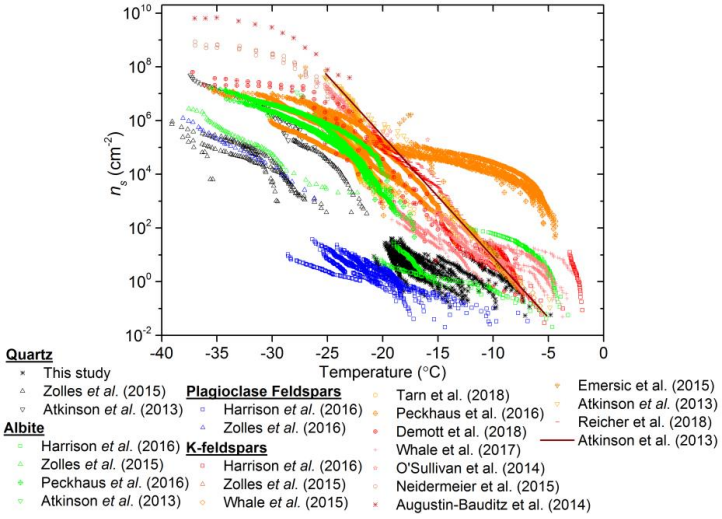

Figure 5: Plot of $n_s(T)$ versus temperature for quartz and feldspar literature data, together with the quartz data from this study.

Atmos. Chem. Phys. Discuss., https://doi.org/10.5194/acp-2019-288
Manuscript under review for journal Atmos. Chem. Phys.
Discussion started: 12 April 2019

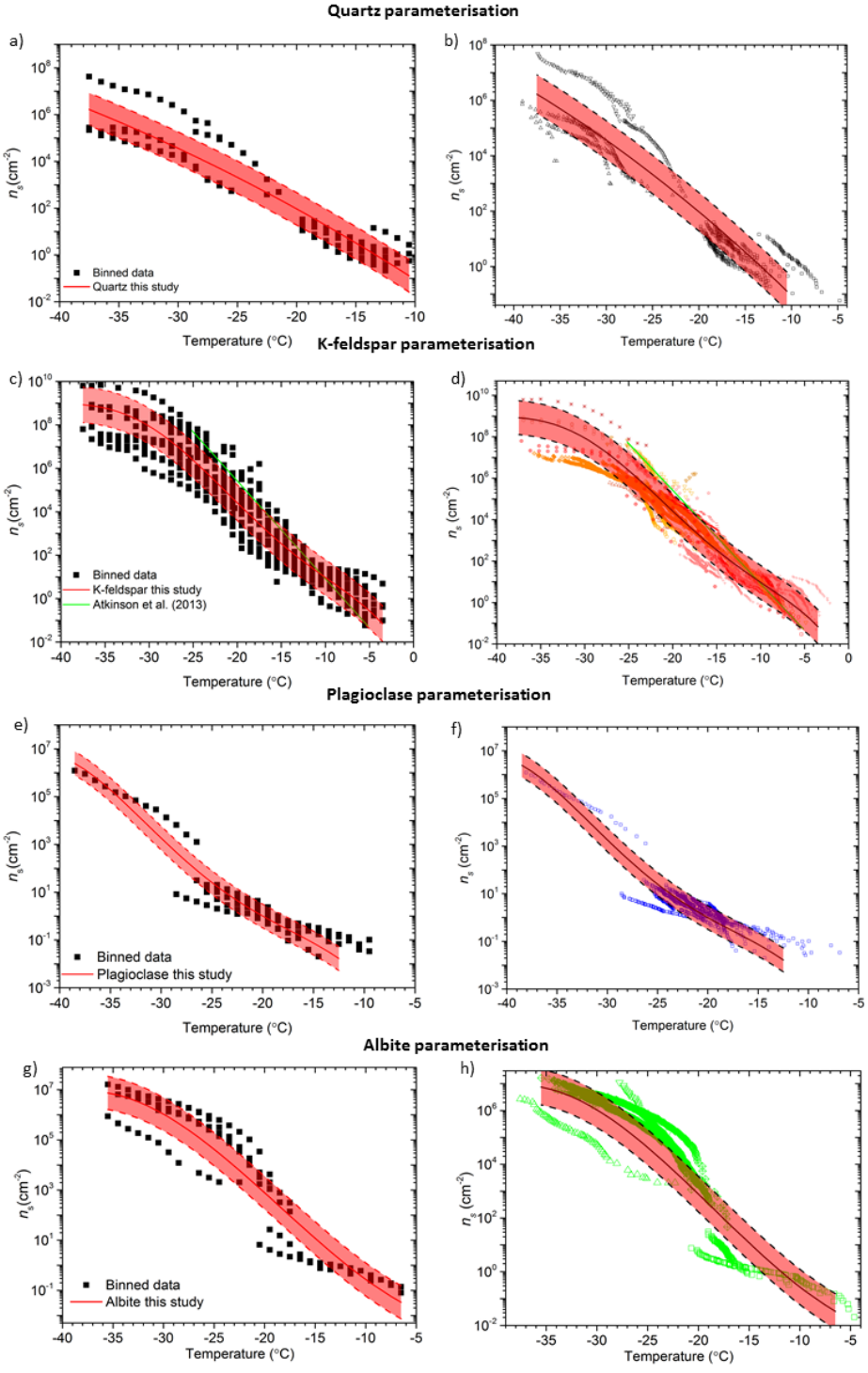

Atmos. Chem. Phys. Discuss., https://doi.org/10.5194/acp-2019-288
Manuscript under review for journal Atmos. Chem. Phys.
Discussion started: 12 April 2019

Atmospheric Chemistry and Physics Discussions

794 **Figure 6:** Parameterisations developed for various silicate minerals using temperature binned literature data. **(a)**
795 Temperature binned data for quartz which was used to calculate the parameterisation with the equation $\log(n_s(T)) = -4.5 + (-3.67E\text{-}1T^1) + (-2.16E\text{-}3T^2)$, valid in the range of -12.5 to -37.5 ˚C with a standard deviation of ± 0.7.**(b)** The newly developed
796
797 parameterisation plotted over the raw quartz data. **(c)** Temperature binned data for K-feldspar which was used to calculate
798 the parameterisation with the equation $\log(n_s(T)) = -3.25 + (-7.93E\text{-}1T^1) + (-6.91E\text{-}2T^2) + (-4.17E\text{-}3T^3) + (-1.05E\text{-}4T^4) + (-9.08E\text{-}7T^5)$, valid in the range of -3.5 to -37.5 ˚C with a standard deviation of ± 0.8. **(d)** The newly developed
799
800 parameterisation plotted over the raw K-feldspar data. **(e)** Temperature binned data for plagioclase feldspars which was used
801 to calculate the parameterisation with the equation $\log(n_s(T)) = (-3.24E\text{-}5T^4) + (-3.17E\text{-}3T^3) + (-1.06E\text{-}1T^2) + (-1.71T) - 12$,
802 valid in the range of -12.5 to -38.5 ˚C with a standard deviation of ± 0.5. **(f)** The newly developed parameterisation plotted
803 over the raw plagioclase data. **(g)** Temperature binned data for albite which was used to calculate the parameterisation with
804 the equation $\log(n_s(T)) = (3.41E\text{-}4T^3) + (1.89E\text{-}2T^2) + (-1.79E\text{-}2T) - 2.29$, valid in the range of -6.5 to -35.5 ˚C with a standard
805 deviation of ± 0.7. **(h)** The newly developed parameterisation plotted over the raw albite data. The standard deviation is
806 highlighted in the red shaded area for each parameterisation and data considered to be unrepresentative of the bulk is
807 excluded from the raw data.

808

809

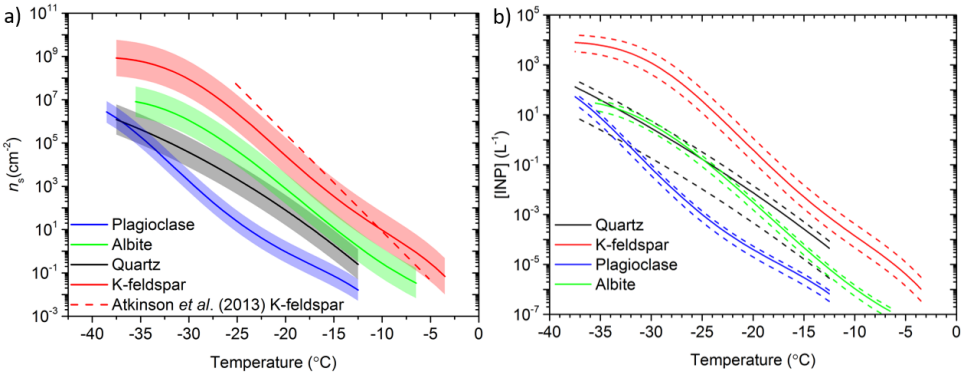

810

811 **Figure 7:** Comparison of the newly developed parameterisations. **(a)** $n_s(T)$ versus temperature for the four newly created
812 parameterisations from this study and the K-feldspar parameterisation proposed by Atkinson et al. (2013). The standard
813 deviation of each parameterisation is shown by the shaded regions. **(b)** INP concentration per litre predictions using the
814 quartz, K-feldspar, albite and plagioclase parameterisations proposed in this study. The solid lines represent the average
815 mineral concentration and the dashed lines represent the upper and lower concentrations based on the variability of mineral
816 concentrations in the atmosphere. An aerosol surface area concentration of 50 µm cm^{-3} and an external mixing assumption
817 were used in the calculation of each prediction.

818

Atmos. Chem. Phys. Discuss., https://doi.org/10.5194/acp-2019-288
Manuscript under review for journal Atmos. Chem. Phys.
Discussion started: 12 April 2019

819

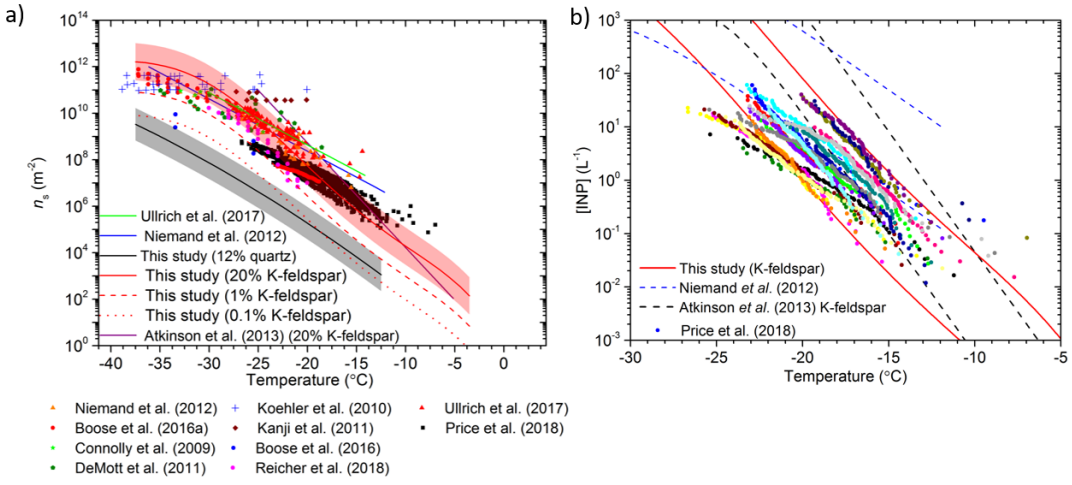

820

821 **Figure 8:** Testing the newly developed K-feldspar and quartz parameterisations against literature data for desert dust. **a)**
822 Comparison of $n_s(T)$ for mineral dust from laboratory and field studies against the K-feldspar and quartz parameterisations.
823 The red lines are $n_s(T)$ values where 0.1, 1 and 20 % of the aerosol surface area is assumed to be K-feldspar. The standard
824 deviation of the K-feldspar parameterisation from this study is represented as the shaded area around the 20 % K-feldspar
825 prediction: this is to show the natural variability in mineral activity. The prediction for 12 % quartz is shown using a black
826 line, with the natural mineral variability highlighted by the shaded region. Literature data and parameterisations have been
827 plotted from (Boose et al., 2016a; Boose et al., 2016b; Connolly et al., 2009; DeMott et al., 2011; Kanji et al., 2011; Koehler
828 et al., 2010; Niemand et al., 2012; Price et al., 2018; Reicher et al., 2018; Ullrich et al., 2017). **b)** Comparison of the INP
829 concentrations predicted by several parameterisations with the INP concentrations measured in the dusty eastern tropical
830 Atlantic region by Price et al. (2018). The predictions were made assuming that 20% of the dust was K-feldspar, consistent
831 with Kandler et al. (2011). For this calculation we assumed that the dust is externally mixed in terms of its mineralogy,
832 although in this regime an internal versus external mixing state assumption makes very little difference (see Atkinson et al.
833 (2013)). The upper and lower bounds of the predicted INP concentrations are based on the lowest and highest aerosol surface
834 area concentrations corresponding to the INP data in Price et al. (2018). Note that the measured INP concentrations from
835 Price et al. (2018) have been corrected downwards by a factor of 2.5 based on the work presented by Price et al. (2018) and
836 Sanchez-Marroquin et al. (in preparation).

837